Biomed Microdevices (2017) 19:33
DOI 10.1007/s10544-017-0162-7

Label-free okadaic acid detection using growth of gold nanoparticles in sensor gaps as a conductive tag

Yuxiang Pan[1,2] · Zijian Wan[1] · Longjie Zhong[1] · Xueqin Li[3] · Qi Wu[3] · Jun Wang[1] · Ping Wang[1,2]

Abstract Okadaic acid (OA) is a marine toxin ingested by shellfish. In this work, a simple, sensitive and label-free gap-based electrical competitive bioassay has been developed for this biotoxin detection. The gap-electrical biosensor is constructed by modifying interdigitated microelectrodes with gold nanoparticles (AuNPs) and using the self-catalytic growth of AuNPs as conductive bridges. In this development, the AuNPs growth is realized in the solution of glucose and chloroauric acid, with glucose oxidation used as the catalysis for growth of the AuNPs. The catalytic reaction product H_2O_2 in turn reduces chloroauric acid to make the AuNPs grow. The conductance signal amplification is directly determined by the growth efficiency of AuNPs and closely related to the catalytic activity of AuNPs upon their interaction with OA molecule and OA aptamer. In the absence of OA molecule, the OA aptamer can absorb onto the surfaces of AuNPs due to electrostatic interaction, and the catalytically active sites of AuNPs are fully blocked. Thus the AuNPs growth would not happen. In contrast, the presence of OA molecule can hinder the interaction of OA aptamer and AuNPs. Then the AuNPs sites are exposed and the catalytic growth induces the conductance signal change. The results demonstrated that developed biosensor was able to specifically respond to OA ranging from 5 ppb to 80 ppb, providing limit of detection of 1 ppb. The strategy is confirmed to be effective for OA detection, which indicates the label-free OA biosensor has great potential to offer promising alternatives to the traditional analytical and immunological methods for OA detection.

Keywords Okadaic acid (OA) · OA aptamer · Gap-based electrical assay · Interdigitated microelectrodes · Label-free biosensor

1 Introduction

Okadaic acid (OA), as the main bioactive compound for diarrheic shellfish poisoning (DSP) toxin, is produced by some unicellular algae from plankton and benthic microalgae. It is a lipophilic, heat-stable phycotoxin which can accumulate in the digestive glands of shellfish without causing any toxic effect on the bivalves. However, when humans consume a sufficient amount of contaminated bivalves, DSP characterized by symptoms such as abdominal pain, nausea, vomiting, and diarrhea can occur (Morton and Donald 1996). Its mechanism of action is based on the inhibition of protein phosphatases (Takai et al. 1992) which play an important role in protein dephosphorylation in cells. Besides, it has been identified that OA is a tumor promoter and has mutagenic and immunotoxic effects. Thus, development of effective methods for OA detection is significant for human health and shellfish industry worldwide.

The mouse bioassay was the reference method recommended by the European Commission (EC) for the detection of OA. However, its drawbacks such as low selectivity, bad reproducibility high cost, and ethical concerns led the demand for alternative methods (Sassolas et al. 2013a). Mass spectrometry

✉ Ping Wang
cnpwang@zju.edu.cn

[1] Biosensor National Special Laboratory, Key Laboratory for Biomedical Engineering of Education Ministry, Department of Biomedical Engineering, Zhejiang University, Hangzhou 310027, People's Republic of China

[2] State Key Laboratory of Transducer Technology, Chinese Academy of Sciences, Shanghai 200050, People's Republic of China

[3] Department of Chemistry, Zhejiang University, Hangzhou 310027, People's Republic of China

Published online: 20 April 2017

(Huang et al. 2014), enzyme inhibition-based assays (Sassolas et al. 2011; Hayat et al. 2012a), immunoassays (Kreuzer et al. 1999; Hayat et al. 2012b), particularly enzyme-linked immunosorbent assay (ELISA) (Sassolas et al. 2013b; Vdovenko et al. 2013; Lu et al. 2012) have been widely developed, among which biosensors including electrochemical enzyme inhibition-based sensor (Volpe et al. 2009) and immunosensor (Campàs et al. 2008; Hayat et al. 2011a) has great appeal because of its rapid response, simple construction and operation, cost-effectiveness, and high sensitivity in OA monitoring. The transducers applied can be surface plasma resonance (Prieto-Simón et al. 2010), piezoelectric (Vaughan et al. 2003), quartz crystal microbalance (Tang et al. 2002), and electrochemical electrodes (Campàs et al. 2008; Hayat et al. 2011a; Hayat et al. 2011b). Electrochemical immunosensors are more favorable due to lower cost of equipment and the convenience of miniaturization.

However, most of the developed OA immunosensors require the use of two antibodies, enzyme or reporter reagents. Since 1990 (Tuerk and Gold 1990; Ellington and Szostak 1990), aptamers have been isolated with high affinity and specificity to a wide range of target analyte. Aptamers as recognition receptors have advantages like easy preparation, low cost, and high stability. Shimaa Eissa et al. (Eissa et al. 2013) selected, identified and characterized DNA aptamers to specifically recognize OA and constructed an aptasensor based on electrochemical impedance spectroscopy. Besides, because of attractive electrical property and good biocompatibility, gold nanoparticles (AuNPs) have been widely used in biomolecular recognition events where sensitive electrical transduction occurs. Especially, AuNPs-based gap-electrical biosensors (Shiigi et al. 2005; Tokonami et al. 2008) have been popularly proposed for low-concentration analyte detection, such as DNA hybridization (Zhang et al. 2013).

In this paper, a label-free competitive bioassay OA detection format sensor is constructed with OA aptamer working as the specifically recognition material for OA molecule, and AuNPs modified in sensor gaps working as a conductive tag. This competitive bioassay format is confirmed to be effective for OA detection, which indicates the label-free OA biosensor has great potential to offer promising alternatives to the traditional analytical and immunological methods for OA detection.

2 Materials and methods

2.1 Chemicals and reagents

All the OA aptamers (5′−/GGTCACCAACAACAGGGAGC GCTACGCGAAGGGTCAATGT GACGTCATGCGGAT GTGTGG/−3′) were purchased from Sangon Biotech (Shanghai, China). OA was purchased from Taiwan Algal Science Inc. The prepared OA stock solution (1 mg/mL in methanol) was stored at −20 °C. (3-Aminopropyl)-triethoxysilane (APTES), glucose, chloroauric acid ($HAuCl_4$), and trisodium citrate were obtained from Sigma-Aldrich and used as received. Other reagents and chemicals were all of analytical grade. All solutions were prepared with ultrapure water. Ultrapure water with electrical resistance of >18.2 MΩ was supplied with Millipore Milli-Q water purification system. Binding buffer, which consists of 50 mM Tris, pH 7.5, 150 mM NaCl, 2 mM $MgCl_2$, was used in OA aptamer dissolvation, dilution and incubation with OA.

2.2 Synthesis of gold nanoparticles

AuNPs were prepared from a reported citrate reduction and stabilization of $HAuCl_4$ method (Grabar et al. 1995) with slight modifications. All glass ware used in these preparations were thoroughly cleaned in aqua regia (HCl/HNO_3 = 3:1 *v*/v), rinsed in triply distilled H_2O, and oven-dried prior to use. In a 100 mL round-bottom flask equipped with reflux, 50 mL $HAuCl_4$ (0.01%) was brought to a rolling boil (110 °C) with vigorous stirring. Rapid addition of 1 mL of sodium citrate (1%) to the vortex of the solution resulted in a color change from pale yellow to burgundy. Boiling was continued for 10 min; the heating device was then removed, and stirring was continued for an additional 15 min, followed by slow cooling to room temperature. The obtained AuNPs solution was stored at 4 °C for future use.

2.3 Sensor fabrication, modification

Interdigitated gold microelectrodes with 30 μm gap were fabricated with standard MEMS technology. A single side polished 4″ N-type silicon wafer (<100>, specific resistance 5–10 Ω cm) with a thickness of 450 μm was used as the substrate. After cleaning with a standard chemical process, a silicon dioxide layer (50 nm) was formed on the polished front side of the wafer through thermal oxidation. Then a Cr/Au layer (30/150 nm) was sequentially sputtered onto the silicon dioxide surface, followed by a photolithography and etching process to define the interdigitated gold microelectrodes and lead wire.

Before assembling AuNPs onto the insulative gap between neighboring comb like gold microelectrodes, a silanization process was performed. The chip was rinsed thoroughly with ethanol to remove possible organic contaminants, followed by immersing it in piranha solution (H_2SO_4/H_2O_2 = 3:1 *v*/v) for 15 min and thoroughly rinsing it with ultrapure water. The cleaned chip was immersed in ethanol with amino-terminating APTES (2.5%) at 4 °C for 6 h, followed by rinsing successively in ethanol and water and blowing with high-purity nitrogen. Then the chip was baked at 110 °C for 30 min to complete the Si-O bond formation (Impens et al.

1999; Brown and Johnson 1997). Subsequently, the silanized chip was immersed in AuNPs colloidal solution at 4 °C for 2 h and washed with ultrapure water. After drying with nitrogen, 20 μL 1 μM OA aptamer in binding buffer was added onto the microelectrodes and incubated for 30 min. Then the chip was washed with binding buffer and stored at 4 °C immersing in binging buffer if not use immediately.

2.4 Sensor measurement procedure

When used for OA detection, the aptamer treated biosensor was incubated with different concentrations of OA in binding buffer for 30 min at 37 °C. Then the sensor was sequentially washed with binding buffer and ultrapure water. Sub sequently, solution containing 150 mM glucose and 300 μM $HAuCl_4$ was applied onto the sensor surface at 37 °C for 2 h. Afterwards, the sensor was rinsed with ultrapure water and dried under nitrogen flow.

All electrochemical or electrical signals were performed with CHI 660 electrochemical workstation (Shanghai, China). Before detection, the sensor was completely dried. Then it was mounted onto the workstation with one electrode pole connected to the working electrode and the other connected to the reference and counter electrodes. By using linear sweep voltammetry (LSV) measurement technology, voltage ranging from −0.3 V to +0.3 V was applied on the working electrode with a scan rate of 1 mV/s and an interval of 1 mV. Then the current-voltage curves can be obtained and the conductance can be calculated according to Ohm's law.

2.5 Sensor measurement principle

The OA biosensor measurement principle is illustrated in Fig. 1. The strategy is based on self-catalytic growth of AuNPs modified in the insulative gap between the comb like gold microelectrodes and the conductance change was used as an indication of interaction between OA molecule and OA aptamer. The biological recognition events are amplified by AuNPs growth. The APTES modification in the preliminary process is aimed to introduce amino group, which facilitates unmodified AuNPs assembling onto the insulative gap area through electrostatic interaction. In the absence of OA molecule, OA aptamers can absorb onto the surfaces of AuNPs due to electrostatic interaction, and the catalytically active sites of AuNPs are fully blocked. In contrast, the presence of OA molecule can hinder the interaction of OA aptamer and AuNPs. Then the AuNPs sites are partially or fully exposed.

Upon the addition of glucose and $HAuCl_4$ solution, the exposed AuNPs sites can be capped with citrate. These active sites will catalytically oxidize glucose in the presence of O_2, producing gluconic acid and H_2O_2, which in turn reduces $AuCl_4^-$ in the solution to grow the exposed AuNPs to Au^0 and enlarge the AuNPs diameters (Wojcieszak et al. 2016). AuNPs work as bridges or even form gold film to conduct the insulative gaps between microelectrodes. The conductance change relies on the growth efficiency of AuNPs and is closely related to the catalytic activity of AuNPs upon their interaction with OA molecule and OA aptamer. Thus the relationship between the conductance signal and the OA concentration can be obtained.

3 Results and discussion

3.1 Characteristics of sensor silanization

Before silanization, chip cleaning is necessary. The method of cleaning should leave the silicon surface smooth, hydrophilic and hydroxylated and therefore appropriate for organosilane deposition. As a strong oxidizing agent, piranha solution reacts violently with organic materials on chip surface, hydroxylate it (add OH groups), and makes it highly hydrophilic. Fig. 2 shows the water contact angle (WCA) after cleaning with piranha solution. It can be seen that the cleaning effect with ethanol is limited (WCA = 43°). After cleaning with piranha solution, the WCA is reduced to 10° or so, which means the hydrophilic on SiO_2 surface is greatly increased. When modified with APTES, the existence of aminopropyl surface groups make WCA increase to 47°, which indicates the successful self-packing of APTES through the OH group on SiO_2 surface.

The thickness of the self-assembled silane film is characterized, as shown in Fig. 3. A silicon wafer with a native oxide layer was used as the substrate. The transparent layer thickness (including oxide layer) of aminopropylsilanated silicon surface was measured by ellipsometry, which is capable of determining the thickness of a thin film covering a reflective substrate. The thickness increases with silanization time. The growth rate is relatively slow within 12 h, especially after 4 h, which is probably indicative of the formation of homogeneous monolayer of aminopropyl silane film. As the process time exceeds 12 h, the film thickness has vigorous growth and shows instability. This may be related with the formation of multilayer of silane films and the loss of unstable layers during washing with ethanol and water before baking. It is suggested that 4 ~ 12 h of silanization is suitable for the formation of stable monolayer of aminopropyl silane film.

3.2 AuNPs modified in sensor gaps

The aminopropylsilanated silicon surface was immersed in AuNPs (diameter 13 nm) colloidal solution at 4 °C for 2 h. Excess AuNPs was removed by rinsing in ultrapure water and then analyzed by SEM. For the aminopropylsilanated silicon surfaces unmodified with AuNPs, or blank silicon surfaces modified with AuNPs, there are no particles retained. In

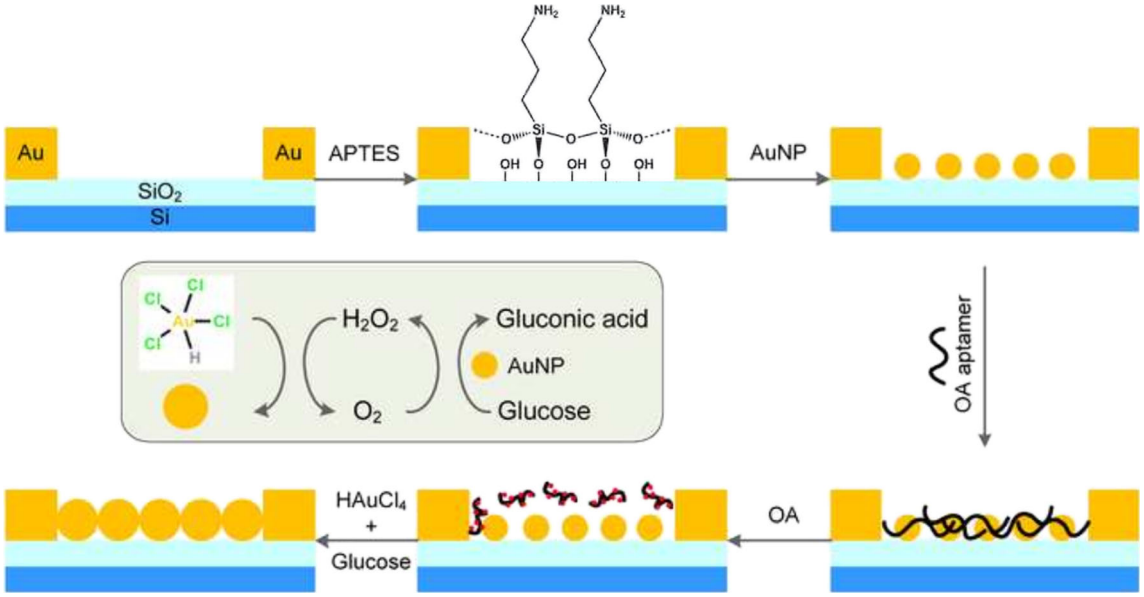

Fig. 1 Schematic diagram of the gap-based electrical biosensor measurement principle

Fig. 4(a ~ c), the modified AuNPs are uniformly distributed, which is related with the homogeneous monolayer of aminopropyl silane film. Meanwhile, the AuNPs density is increasing because of the raising of aminopropyl group number. When the silanization time exceeds 10 h (Fig. 4d), the gold nano clusters start to appear in the local area, and the dispersed particles are largely reduced. After more than 16 h (Fig. 4e), the AuNPs are aggregated intensively and form a multi-layer structure. After 24 h (Fig. 4f), the AuNPs connect with each other and make the gap conductive between neighboring comb like microelectrodes. So, considering the experimental results in Figs. 3 and 4, 6h is chosen as the silanization time in the further experiments. Thus, a stable monolayer of silane film can be obtained, and uniformly dispersed AuNPs with high density can be modified on it.

3.3 Characterization of AuNPs growth

As the measurement mechanism is based on the self-catalytic AuNPs growth, several tests are preliminarily carried out to verify the validity of AuNPs growth in glucose and $HAuCl_4$ solution, and evaluate the distinctiveness of the signal intensity after every step of process. The morphology alteration on sensor surface after AuNPs growth is characterized by SEM. As shown in Fig. 5(a), after growing for 2 h, the AuNPs size increase from 13 nm to around 100 nm, and the shape change into partially triangle or polygon, which indicates the chemical reduction of $AuCl_4^-$ on AuNPs surfaces and a certain randomness of the growth in static solution. In Fig. 5(b), the large area with higher brightness indicates the comb like microelectrodes. The AuNPs are widely dispersed in the insulative gap with greater particle size and smaller spacing between particles.

In Fig. 5(c), current-voltage curves for blank sensor, sensor modified with APTES followed by AuNPs immobilization, and after 2 h of self-catalytic AuNPs growth are measured by LSV technology. According to Ohm's law, the current through two poles of electrodes is proportional to the voltage applied on them, and the slope of the curve is calculated as the conductance. The conductance before AuNPs growth (5.17 nS) is slightly increased in comparison with the blank sensor (approximate zero), which indicates the interparticle distance

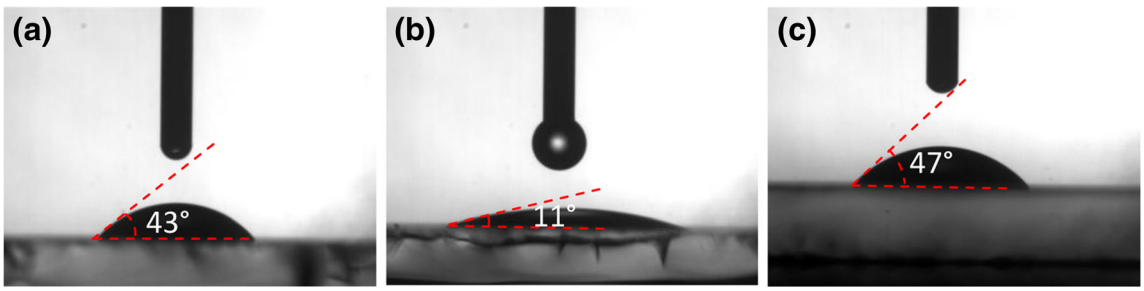

Fig. 2 WCA measured before and after silanization on glass surfaces. **a** WCA measured after ethonal washing; **b** WCA measured after cleaning with piranha solution; **c** WCA measured after silanization with APTES (4 °C, 6 h)

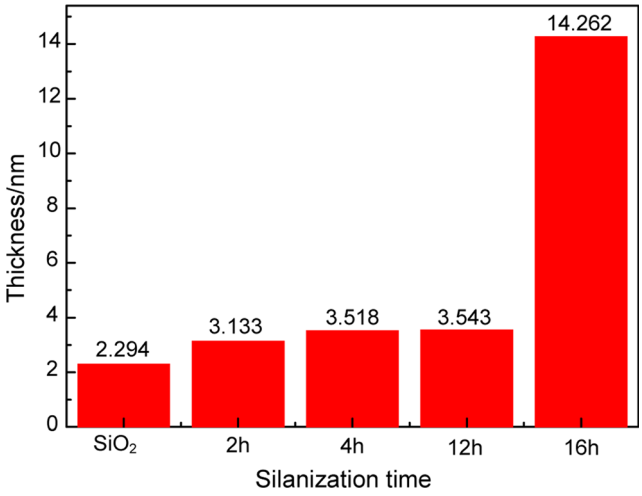

Fig. 3 Ellipsometricly measured transparent layer thickness (including oxide) of aminopropylsilanated silicon surface and its growth with silanization time (under 4 °C)

between AuNPs is too large to change the insulativity of the gap. After AuNPs growing, the conductance (102.24 nS) is increased by around 20 times, which means the electron tunneling path formation is facilitated between the microelectrodes.

3.4 Gap-based electrical OA assay

The developed gap-based electrical detection strategy was tested using OA aptamer and OA molecule. Typical conductance signals are presented in Fig. 6(a). All the current-voltage curves (not shown) exhibit good linearity in the potential range, indicating that the microelectrodes behave as ideal physical resistors under the experimental conditions. When the AuNPs modified sensor are treated with OA aptamer and the subsequent solution containing 20 ppb OA, the conductance signals get very close to that of AuNPs modified sensor. After growing in glucose and $HAuCl_4$ solution, the AuNPs, AuNPs/aptamer, and AuNPs/aptamer/OA sensor signals show obvious distinction. As expected, the largest current is observed for the AuNPs sensor with growing. The current signal for AuNPs/aptamer/OA sensor with growing is larger than that of AuNPs/aptamer sensor with growing, indicating that the binding of OA and aptamer exhibit weaker affinity with AuNPs than aptamer, resulting in the enlargement of AuNPs and facilitating the electron transfer between microelectrodes.

In order to reveal the effect of interaction of OA and aptamer on AuNPs growing more clearly, an electrochemical impedance spectroscopy (EIS) measurement was carried out, as Shimaa Eissa et al. did (Eissa et al. 2013). Disulfide terminated aptamer (5′HO-$(CH_2)_6$-S-S-$(CH_2)_6$/GGTCACCAACAACAGGGAGC GCTACGCGAAGGGTCAATGTGACGTCATGCGGATGT GTGG/−3′) (1 μM) was immobilized on the gold microelectrodes through self-assembly technique. Then 1 mM 6-mercato-1-hexanol (MCH) was self-assembled on the microelectrodes surface to block further possible nonspecific adsorption on the electrodes. OA was applied onto the aptamer-modified microelectrodes and incubated for 30 min. The EIS was performed with 5 mM $[Fe(CN)_6]^{4-/3-}$ redox couple in PBS, pH 7.4, using a frequency range of 1 ~ 10^5 Hz, and ac amplitude of 5 mV. Fig. 6(b) shows the Nyquist plots. In the spectrum, the

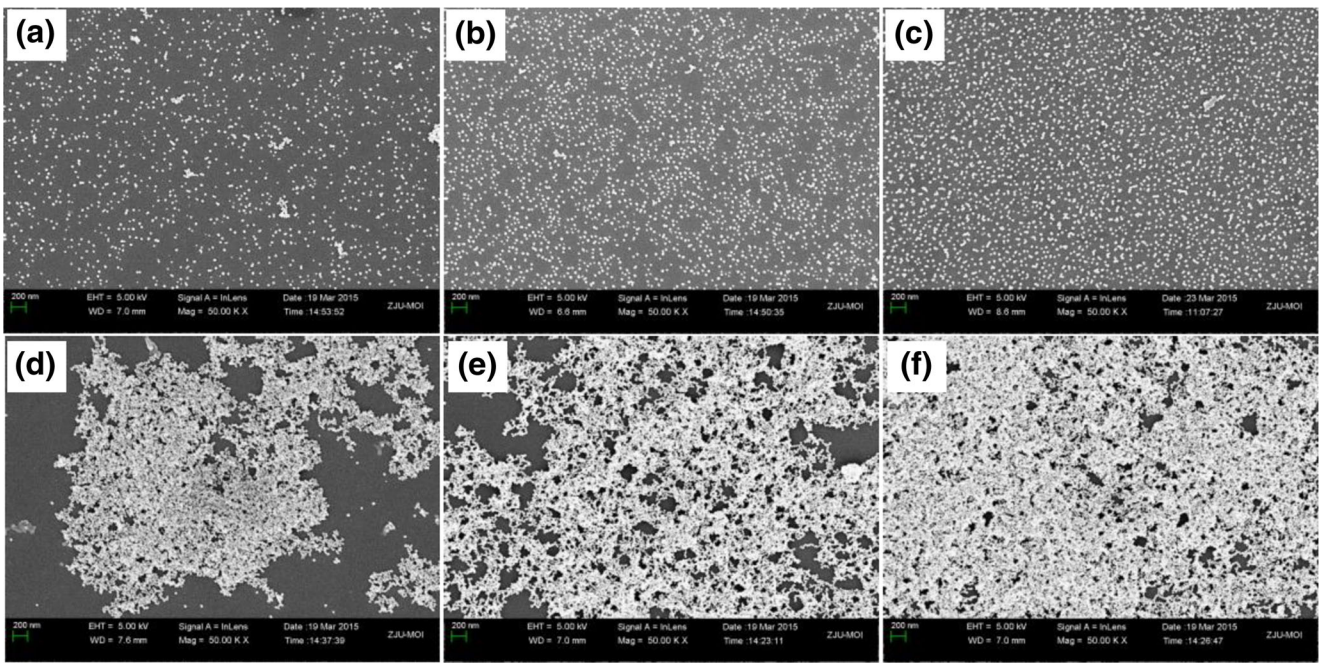

Fig. 4 SEM images of aminopropylsilanated silicon surface after immersing in AuNPs at 4 °C for 2 h, magnification 50,000×. The silanization time is: **a** 2 h; **b** 4 h; **c** 6 h; **d** 10 h; **e** 16 h; **f** 24 h

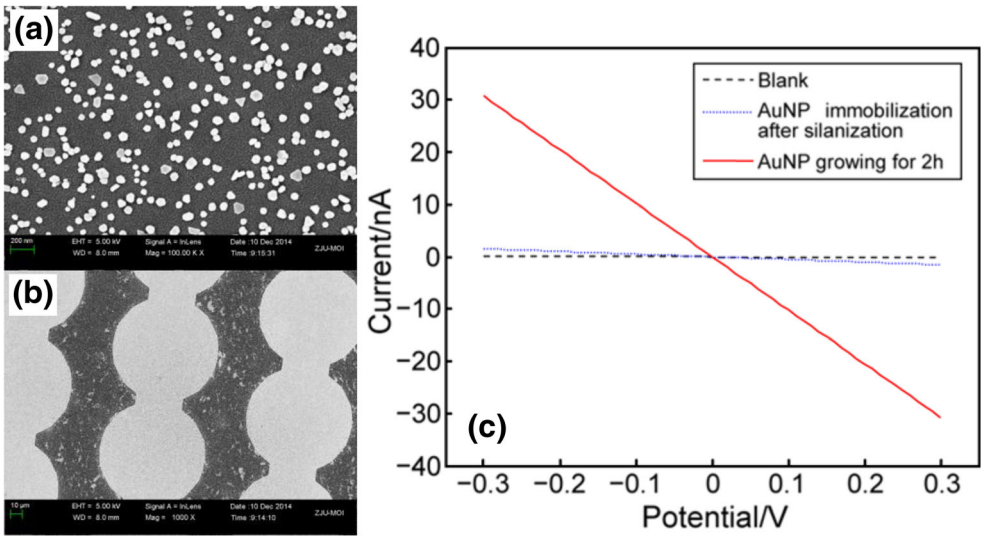

Fig. 5 Characterization of AuNPs growth after 2 h incubation in 150 mM glucose and 300 μM $HAuCl_4$ solution at 37 °C. *SEM* images of sensor morphology with magnification of 100,000× **a** and 1000× **b**. **c** Comparison of the current-voltage curves measured before and after AuNPs growing

semicircular part in a high frequency region corresponds to the electron-transfer process, and the semicircle diameter corresponds to the charge-transfer resistance (R_{ct}). The electron-transfer process is fast on bare interdigitated electrode. R_{ct} for aptamer-modified electrode increases, indicating a hindered electron-transfer process. The self-assembled MCH fill the exposed gold areas and induces a larger R_{ct}. The binding of OA onto aptamer introduces a large drop in R_{ct}, which is related with the conformational change of the aptamer to a more compact structure. It can be noted that the facilitation of AuNPs growing for AuNPs/aptamer/OA sensor comparing with AuNPs/aptamer sensor is probably due to the conformational change of aptamer and the induced affinity change with AuNPs.

OA with different concentrations were measured using this strategy. As expected, with increasing number of OA molecules, the affinity of OA binding aptamer with AuNPs is weakened, resulting in a large degree of AuNPs growth and then a more substantial current. The sensor response is quantified as $(S - S_0)/S_0$ to obtain better consistency between different channels of the interdigitated array microelectrodes, where S_0 corresponds to the conductance value before AuNPs growing and S corresponds to that of after AuNPs growing. Fig. 7 shows the linear relationship between $(S - S_0)/S_0$ and OA concentration in the range of 5 ppb ~ 80 ppb, with a correlation coefficient of 0.9916 and a detection limit of 1 ppb.

As a sensing device for measuring OA, it may face the potential interferences arising from the other DSP toxins that have similar structure. In order to improve the selectivity of this sensing device, we chose OA34 aptamer as specifically recognition material for OA molecule, which showed remarkable sensitivity and selectivity for OA against DTX-1 and DTX-2 (Eissa et al. 2013).

4 Conclusions

A novel gap-based electrical biosensor is constructed for label-free OA detection. The strategy is based on the signal amplification after self-catalytic growth of modified AuNPs in gaps between microelectrodes which functions as a

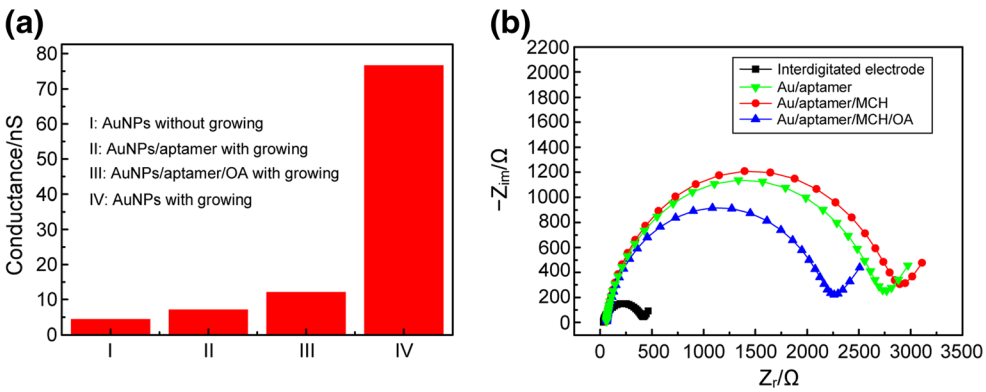

Fig. 6 Electrical and electrochemical performance of aptasensor based on the interaction of OA and aptamer. **a** Different degrees of enlargement of conductance signal after AuNPs growing for AuNPs, AuNPs/aptamer, and AuNPs/aptamer/OA; **b** Nyquist plots of 5 mM $[Fe(CN)_6]^{4-/3-}$ redox couple in PBS, pH 7.4, for bare interdigitated gold microelectrode, Au/aptamer, Au/aptamer/MCH, and after binding with 20 ppb OA

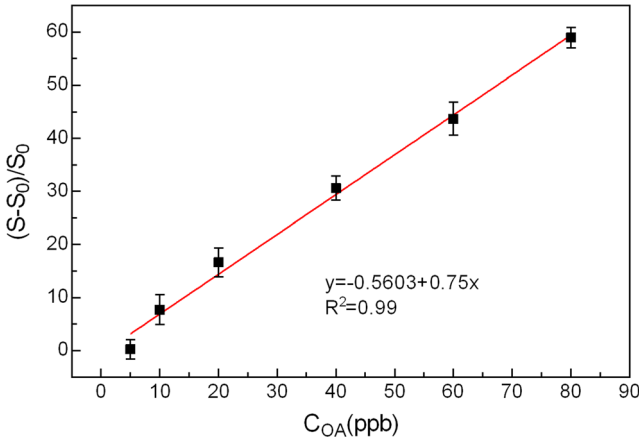

Fig. 7 A typical linear fitting calibration curve for OA, plot of $(S - S_0)/S_0$ vs OA concentration. All the data are represented by means ± SD (standard deviation), $n = 3$

conductive tag. The processes of silanization, AuNPs immobilization and AuNPs growth are characterized. The surface-immobilized AuNPs exhibit excellent self-catalytic activity. The variation of the catalytic activity of AuNPs upon binding of OA with aptamer is exploited. The strategy is verified to be feasible for quantitative OA analysis through OA binding induced conformational change within the aptamer and the succeeding conductance variation induced by AuNPs growing. The experimental results show that the biosensor has dynamic responses to OA with different concentrations. With ease of fabrication and miniaturization, the gap-based electrical biosensor has great potential in large sample and high throughput OA detection.

Acknowledgements This work was supported by Major International Cooperation Project of Natural Science Foundation of China (No. 61320106002), Marine Public Welfare Project of China (No.201305010), and Natural Science Foundation of China (No. 31228008, 81501553).

References

T.S.D. Brown, B.F. Johnson, Nucleation and growth of nano-gold colloidal lattices. Chem. Commun. **11**, 1007–1008 (1997)

M. Campàs et al., Enzymatic recycling-based amperometric immunosensor for the ultrasensitive detection of okadaic acid in shellfish. Biosens. Bioelectron. **24**(4), 716–722 (2008)

S. Eissa et al., Selection and identification of DNA aptamers against okadaic acid for Biosensing application. Anal. Chem. **85**(24), 11794–11801 (2013)

A.D. Ellington, J.W. Szostak, In vitro selection of RNA molecules that bind specific ligands. Nature **346**(6287), 818–822 (1990)

K.C. Grabar et al., Preparation and characterization of Au colloid monolayers. Anal. Chem. **67**(4), 735–743 (1995)

A. Hayat, L. Barthelmebs, J.-L. Marty, Enzyme-linked immunosensor based on super paramagnetic nanobeads for easy and rapid detection of okadaic acid. Anal. Chim. Acta **690**(2), 248–252 (2011a)

A. Hayat et al., An electrochemical immunosensor based on covalent immobilization of okadaic acid onto screen printed carbon electrode via diazotization-coupling reaction. Talanta **85**(1), 513–518 (2011b)

A. Hayat, L. Barthelmebs, J.-L. Marty, A simple colorimetric enzymatic-assay for okadaic acid detection based on the immobilization of protein phosphatase 2A in sol-gel. Appl. Biochem. Biotechnol. **166**(1), 47–56 (2012a)

A. Hayat et al., Development of a novel label-free amperometric immunosensor for the detection of okadaic acid. Anal. Chim. Acta **724**, 92–97 (2012b)

H. Huang et al., Determination of okadaic acid and Dinophysistoxin-1 in mussels by high-performance liquid chromatography–tandem mass spectrometry. Anal. Lett. **47**(12), 1987–1994 (2014)

N. Impens, P. Van Der Voort, E. Vansant, Silylation of micro-, meso-and non-porous oxides: A review. Microporous Mesoporous Mater. **28**(2), 217–232 (1999)

M.P. Kreuzer, C.K. O'Sulliva, G.G. Guilbault, Development of an ultrasensitive immunoassay for rapid measurement of okadaic acid and its isomers. Anal. Chem. **71**(19), 4198–4202 (1999)

S.-Y. Lu et al., Production of monoclonal antibody and application in indirect competitive ELISA for detecting okadaic acid and dinophytoxin-1 in seafood. Environ. Sci. Pollut. Res. **19**(7), 2619–2626 (2012)

S.L. Morton, R.T. Donald, Determination of okadaic acid content of dinoflagellate cells: A comparison of the HPLC-fluorescent method and two monoclonal antibody ELISA test kits. Toxicon **34**(8), 947–954 (1996)

B. Prieto-Simón et al., High-sensitive flow-based kinetic exclusion assay for okadaic acid assessment in shellfish samples. Biosens. Bioelectron. **25**(6), 1395–1401 (2010)

A. Sassolas et al., Development of an efficient protein phosphatase-based colorimetric test for okadaic acid detection. Anal. Chim. Acta **702**(2), 262–268 (2011)

A. Sassolas et al., Detection of the marine toxin okadaic acid: Assessing seafood safety. Talanta **105**, 306–316 (2013a)

A. Sassolas et al., Improvement of the efficiency and simplification of ELISA tests for rapid and ultrasensitive detection of okadaic acid in shellfish. Food Control **30**(1), 144–149 (2013b)

H. Shiigi et al., Label-free electronic detection of DNA-hybridization on Nanogapped gold particle film. J. Am. Chem. Soc. **127**(10), 3280–3281 (2005)

A. Takai et al., Inhibitory effect of okadaic acid derivatives on protein phosphatases. A study on structure-affinity relationship. Biochem. J. **284**, 539–544 (1992)

A.X.J. Tang et al., Immunosensor for okadaic acid using quartz crystal microbalance. Anal. Chim. Acta **471**(1), 33–40 (2002)

S. Tokonami, H. Shiigi, T. Nagaoka, Open bridge-structured gold nanoparticle Array for label-free DNA detection. Anal. Chem. **80**(21), 8071–8075 (2008)

C. Tuerk, L. Gold, Systematic evolution of ligands by exponential enrichment: RNA ligands to bacteriophage T4 DNA polymerase. Science **249**(4968), 505–510 (1990)

R.D. Vaughan et al., Piezoelectric immunosensors for environmental monitoring. Int. J. Environ. Anal. Chem. **83**(7–8), 555–571 (2003)

M.M. Vdovenko et al., Determination of okadaic acid in shellfish by using a novel chemiluminescent enzyme-linked immunosorbent assay method. Talanta **116**, 343–346 (2013)

G. Volpe et al., A bienzyme electrochemical probe for flow injection analysis of okadaic acid based on protein phosphatase-2A inhibition: An optimization study. Anal. Biochem. **385**(1), 50–56 (2009)

R. Wojcieszak et al., Selective oxidation of glucose to glucuronic acid by cesium-promoted gold nanoparticle catalyst. J. Mol. Catal. A Chem. **422**, 35–42 (2016)

J. Zhang et al., Self-catalytic growth of unmodified gold nanoparticles as conductive bridges mediated gap-electrical signal transduction for DNA hybridization detection. Anal. Chem. **86**(2), 1178–1185 (2013)